Photofission and photoneutron cross sections and photofission neutron multiplicities for ^{233}U, ^{234}U, ^{237}Np, and ^{239}Pu

B. L. Berman
Department of Physics, The George Washington University, Washington, D.C. 20052

J. T. Caldwell and E. J. Dowdy
Los Alamos National Laboratory, University of California, Los Alamos, New Mexico 87545

S. S. Dietrich, P. Meyer, and R. A. Alvarez
Lawrence Livermore National Laboratory, University of California, Livermore, California 94550
(Received 18 August 1986)

The photonuclear cross sections for ^{233}U, ^{234}U, ^{237}Np, and ^{239}Pu have been measured from threshold up to 18 MeV. The source of radiation was the monoenergetic photon beam from the annihilation in flight of fast positrons. The branching among the neutron-producing reaction channels was determined by measuring the photofission prompt neutron multiplicities $\bar{\nu}_p$. One interesting result is the complete absence of any (γ,2n) cross section for ^{233}U and ^{234}U. The values of $\bar{\nu}_p(E)$ for ^{234}U agree with those measured with neutrons incident on ^{233}U. The parameters of the giant dipole resonance deduced from the total photonuclear cross sections show that these nuclei have large static deformations, as expected. The integrated photofission cross sections are large (as are the absolute fission probabilities), and account for 60% to 80% of the total photonuclear absorption strength.

I. INTRODUCTION

As pointed out by Bohr,[1] photofission reactions make use of the relative simplicity and directness of the electromagnetic interaction as a powerful tool with which to explore the process of nuclear fission. However, owing to the difficulty of performing photofission measurements, especially with monoenergetic photons, very little accurate, detailed, and systematic data have been obtained. We have made a systematic study of the photonuclear process in ^{232}Th, ^{233,234,235,236,238}U, ^{237}Np, and ^{239}Pu, the last part of which is reported here, in an effort to provide such data.

Work in the photofission field through the mid-1970s is summarized in the review articles by Huizenga and Britt[2] and by Bhandari and Nascimento,[3] and is set in the framework of fission research in the book of Vandenbosch and Huizenga.[4]

The characteristics of the giant dipole resonance (GDR) for the actinide nuclei and the deformation parameters of these nuclei are of particular interest. For such high-Z, high-Coulomb-barrier nuclei, the total photonuclear cross section $\sigma(\gamma,\text{tot})$, from which one can determine the (static) deformation parameters,[5,6] is, to a good approximation, equal to the sum of the photoneutron and photofission cross sections.

We have published the results of the first half of our systematic study, on ^{235}U, ^{236}U, ^{238}U, and ^{232}Th, previously.[7,8] Most of the details of the experimental apparatus and techniques and the data-analysis procedures can be found in these papers; only those features specific to the present results (such as the sample characteristics, backgrounds, and certain newly developed analysis techniques) will be discussed in detail here.

We do wish to reemphasize, however, that we have measured the important properties of the fission process, namely the average prompt neutron multiplicity $\bar{\nu}_p(E)$, the ratio of the neutron and fission widths Γ_n/Γ_f as a function of the fissionability Z^2/A, and the fission probability $P_f(E)$, as well as the important nuclear properties of the actinides, particularly their deformation characteristics, that are determined from $\sigma(\gamma,\text{tot})$. We wish to point out as well that the analysis of the cross-section data here depends upon the ability to assign the detected reaction events to the various photoneutron and photofission channels based upon their measured neutron multiplicity and average neutron energy. These, in turn, depend on the values employed for $\bar{\nu}_p$. In this experiment the values for $\bar{\nu}_p$ were measured, not assumed, as has been done in the only previous work of this kind.[9]

Previous experimental cross-section work for the actinide nuclei studied here usually has fallen into one of two categories: (1) measurements at excitation energies in the GDR region, and (2) measurements in the low-energy region near the fission barriers and (γ,n) thresholds. For the GDR energy region, there have been only two bremsstrahlung measurements reported, namely the very old photofission measurement of Katz *et al.*[10] on ^{233}U, ^{237}Np, and ^{239}Pu, and the more recent photon-absorption measurement of Gurevich *et al.*[11] on ^{239}Pu, and only one measurement with monoenergetic (positron-annihilation) photons, by Veyssière *et al.*,[9] on ^{237}Np. (Comparison of the results of Refs. 9 and 11 for ^{235}U, ^{238}U, and ^{232}Th with our previous results can be found in Ref. 7.)

For the low-energy region, data have been published previously by Huizenga *et al.*[12] for ^{233}U, ^{234}U, and ^{237}Np; by Ostapenko *et al.*[13] for ^{233}U, ^{237}Np, and ^{239}Pu; by Lindgren *et al.*[14,15] for ^{234}U; by Geraldo *et al.*[16] for

^{237}Np; and by Shapiro and Stubbins[17] and Dragnev et al.[18] for ^{239}Pu.

Photofission $\bar{\nu}_p$ data obtained with low-energy bremsstrahlung have been published by two of us[19] for all of the nuclei studied here; no other such data have been reported. Relatively recent $\bar{\nu}_p$ data for neutron-induced fission have been obtained for ^{233}U + n (^{233}U + n corresponds here to ^{234}U+γ) by Manero and Konshin,[20] Boldeman et al.,[21] and Gwin et al.,[22] and for ^{232}U + n and ^{238}Pu + n by Jaffey and Lerner.[23]

II. EXPERIMENT AND DATA REDUCTION

The experimental method and data-reduction techniques employed in the present measurements are based on those used in our other photonuclear and photofission experiments. A detailed description appears in Refs. 7, 8, and 19 (and earlier references therein).

Briefly, the method consists of using a positron beam from the LLNL Electron-Positron Linear Accelerator incident upon a low-Z target to produce photons by annihilation in flight. The collimated photon beam passes through a xenon-filled spherical ion chamber, which serves as a flux monitor, and impinges on the photofission sample under study that is located at the center of a high-efficiency 4π neutron detector. The neutron detector consists of 48 BF_3 tubes embedded in a 61-cm cube of paraffin and arranged in four concentric rings. The ratio of counting rates in the outer and inner rings (the ring ratio) is a sensitive function of the average neutron energy. In the present experiment the photon energy resolution ranged from about 250 keV at energies below 10 MeV to about 325 keV at the highest energy ($\approx$18 MeV).

The photofission samples were located at a distance of 310 cm from the annihilation target. Up to eight samples or blanks, including a standard Pu-Be neutron source used to monitor the detector efficiency, were loaded into the neutron detector sequentially with a remotely controlled sample changer, so that beam-tuning conditions remained the same for different samples at a given energy. The actinide sample specifications are given in Table I; the photonuclear thresholds[4,24] for these nuclei are listed in Table II. The photonuclear thresholds determined in the present experiment [in particular, that for ^{237}Np(γ,2n)] agree, within the experimental limits, with those given in Table II.

Because the ^{233}U, ^{237}Np, and ^{239}Pu samples were encapsulated in metal cans (see Table I), background subtractions for (γ,1n) events required a knowledge of the photoneutron cross sections for copper and nickel; these were obtained from the results published in Refs. 25 and 26, respectively.

The absolute calibration of the photon beam flux was accomplished by comparing the response of the ion chamber with that of a large (20$\times$20 cm) NaI crystal. This calibration has been done periodically (e.g., see Ref. 27), and has remained remarkably constant over a period of over 20 years.

As a check on all aspects of the experimental calibration and monitoring, a sample of ^{141}Pr was used along with the actinide samples, and the absolute cross section obtained was compared with the results of previous measurements.[28–31] The total photoneutron cross section for ^{141}Pr determined here is shown (as the data points) in Fig. 1. The average of the four previous determinations done with monoenergetic photons, which all lie within a few percent of each other, is shown as the curve in the figure. It is clear that the agreement is excellent. Moreover, a very recent determination, also done at Lawrence Livermore National Laboratory,[32] is in excellent agreement as well.

Certain special procedures were employed in the reduction of the present data, for various reasons. For these photoreaction experiments, the neutron-multiplicity counting technique was modified to account simultaneously and independently for (γ,n), (γ,2n), and (γ,F) events. But because ^{233}U and ^{239}Pu are fissile, special care had to be taken to avoid overestimating the photofission cross section because of fission events initiated by moderated photoneutrons and fission neutrons. This was accomplished by three techniques, two experimental and one calculational. First, some data were obtained both with and without cadmium foil wrapped around the samples; the cadmium foil virtually eliminated the slow-neutron fission, but increased greatly the single-photoneutron background. Second, both large and small samples were used for ^{233}U and ^{239}Pu (and also for ^{234}U), not only to keep the counting rates within reasonable bounds, but also so that the multiplication corrections which must be applied would be different for the two samples. Thus, where data for both samples were obtained for a common photon energy, an automatic cross-

TABLE I. Sample characteristics.

Sample	Physical description	Mass (g)	Purity (%)
^{233}U	(1) Metal disks in brass can, 1.91 cm diam	40.31	97.46
	(2) Metal disks in brass can, 1.91 cm diam	101.06	97.46
^{234}U	(1) Oxide powder in Lucite cylinder, 2.54 cm diam	3.325	99.84
	(2) Oxide powder in Lucite cylinder, 2.54 cm diam	12.525	99.78
^{237}Np	Metal in brass cylinder, 2.86 cm diam	45.62	100.00
^{239}Pu	(1) Metal disk in nickel can, 2.29 cm diam	4.98	97.67
	(2) Metal cube in steel can, 1.25 cm edge length	29.91	99.92

TABLE II. Photoneutron thresholds and photofission barriers (in MeV).

Nucleus	$E_{\text{thr}}(\gamma,\text{n})$[a]	$E_{\text{thr}}(\gamma,2\text{n})$[a]	$B_F(\gamma,f)$[b]
^{233}U	5.753	13.010	5.7±0.3
^{234}U	6.844	12.597	6.0±0.2
^{237}Np	6.628	12.310	5.6±0.3
^{239}Pu	5.647	12.645	5.8±0.2

[a]From Ref. 24.
[b]From Ref. 4, p. 255.

check would result. Finally, a new fission-multiplication-correction program was developed and used in the data-reduction procedure. The fact that all of these methods converged (while the uncorrected data diverged significantly) gives us confidence that this effect was accounted for correctly.

Another problem arose because the small samples or small cross sections led to certain results having poor statistical quality. The method by which $\bar{\nu}_p(E)$ is determined from the observed neutron multiplicity at each photon energy is discussed in detail in Refs. 8 and 19. Here, however, for those cases where the ring-ratio data were not adequate to determine the neutron detector efficiency for photofission events to be used in the computation of $\bar{\nu}_p(E)$ and the associated multiplicity width parameter $\Sigma(E)$, the *relative* energy-dependent efficiency (normalized appropriately) for ^{236}U (see Ref. 8) was substituted. Also, straight-line fits to the $\bar{\nu}_p$ data (see Sec. III A) were used for the cross-section analysis. Finally, it turned out (remarkably enough; see below) that the $(\gamma,2\text{n})$ cross sections determined in this way for ^{233}U and ^{234}U are consistent with zero up to the highest energies measured here. Therefore, these cross sections were set identically equal to zero in an iterated analysis in order to reduce the error bars appropriately for the other cross sections for these nuclei.

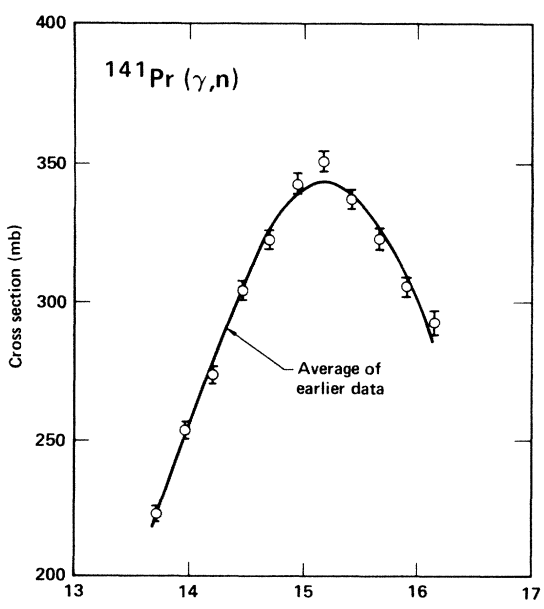

FIG. 1. Total photoneutron cross section for ^{141}Pr measured during the present experiment (data points), compared with the fitted average of four previous measurements also done with monoenergetic photons.

Further details of the data-analysis procedures and discussions of the experimental uncertainties are given in detail elsewhere.[5,7,8,26,27] Statistical uncertainties are reflected in the error bars on the data points. Systematic uncertainties arising from the subtraction of the positron-bremsstrahlung yields, from the neutron-detector efficiency calibration, and from the photon-flux calibration are about 2%, 3%, and 5%, respectively. Impurities in the samples (see Table I) have been accounted for whenever their effect on the results exceeded 1%. Uncertainties resulting from multiplication effects in the samples are estimated to be less than 2%; those resulting from subtraction of the copper and nickel backgrounds from the $(\gamma,1\text{n})$ cross sections are estimated to be less than 5% for ^{233}U and ^{237}Np and less than 10% for ^{239}Pu (at the highest energies, for the single-photoneutron cross section only). The final (γ,F) and (γ,tot) cross-section values are subject to overall systematic uncertainties that do not exceed 7%. The statistical uncertainties for the total photonuclear cross sections were computed by adding in quadrature those for the partial cross sections.

III. RESULTS AND DISCUSSION

A. Photofission neutron multiplicities and width parameters

The values determined here for the prompt-neutron-multiplicity width parameter $\Sigma(E)$ and the average number of prompt neutrons per photofission $\bar{\nu}_p(E)$ are given in Table III, in the form of the slopes and intercepts of straight-line fits to the data. Because of their relatively large statistical uncertainties, the data for $\Sigma(E)$ for ^{234}U and ^{237}Np were fitted by constant (energy-independent) values.

The $\bar{\nu}_p(E)$ data are shown in Fig. 2. Although there are hints of structure in the energy dependence of $\bar{\nu}_p$, especially for ^{237}Np and ^{239}Pu near 12–13 MeV, it is our judgment that, because of the statistical uncertainties and the scatter of the data points and because of the lack of any corroborating data from other kinds of experiments, a definite claim of anything other than a smooth, monotonically increasing dependence of $\bar{\nu}_p$ on energy cannot be justified at this time. [This is in contrast with the case for ^{232}Th (see Ref. 8).] Therefore, we fitted the $\bar{\nu}_p$ data with straight lines as shown in Fig. 2 and as specified in Table III. Strong evidence that this procedure is reasonable is given by the high values for the correlation coefficients, also given in Table III. Although the average value for the slope of $\bar{\nu}_p(E)$ is reasonable (0.177, or one neutron per 5.64 MeV), the slope for ^{234}U is considerably shallower and that for ^{237}Np is considerably steeper than this average value. These slopes, of course, will be reflected in the energy dependence of the average kinetic energy of the fission fragments.

TABLE III. Multiplicity width parameter $\Sigma(E)$ and average number of prompt neutrons per photofission $\bar{\nu}_p(E)$.

Nucleus	$\Sigma(E)$	$\bar{\nu}_p(E)$[a]	CC[b]
^{233}U	$0.249E+1.128$	$0.1693E+1.194$	0.973
^{234}U	1.30[c]	$0.1326E+1.582$	0.922
^{237}Np	1.40[c]	$0.2266E+0.977$	0.976
^{239}Pu	$0.0481E+0.794$	$0.1803E+1.760$	0.908

[a]Least-squares fit.
[b]Correlation coefficient.
[c]For ^{234}U and ^{237}Np the data for Σ were best fitted by a constant value.

Our values for $\bar{\nu}_p$ at $E=8.5$ MeV are compared in Table IV with those from the bremsstrahlung data of Ref. 19. It is seen that the overall agreement is excellent, except possibly for the case of ^{237}Np; the higher value determined in the present work owes its origin to the relatively high (and constant) value for Σ used here.

When the same compound nucleus is formed during neutron-induced fission, we can compare our photofission $\bar{\nu}_p$ values with those determined using incident neutrons. For thermal neutrons, values of $\bar{\nu}_p$ for three of the four nuclei studied here have been measured. These are compared with our values and also with the calculated values of Yamamoto and Sugiyama[33] in Table V. For the well-determined case of ^{234}U (formed by ^{233}U + n), the values are all in superb agreement. For ^{239}Pu, the agreement with the value for ^{238}Pu + n (Ref. 23) is good. But for ^{233}U, the value for ^{232}U + n (from the same reference) is in violent disagreement with our value (it is many standard deviations too high). The calculated value[33] of $\bar{\nu}_p$ for ^{233}U lies 17% higher than our measured one, but the value from Ref. 23 is 24% higher than even this calculated one.

The only case studied here for which the energy dependence of $\bar{\nu}_p$ has been measured with neutrons is that of ^{234}U (^{233}U + n). The results of Refs. 20 and 21 are compared with the present results in Fig. 3. Although they lie somewhat lower than the present photofission results, our experimental uncertainties are such that we can call the agreement good. This did not have to be the case, of course. If, for example, the angular-momentum dependence of $\bar{\nu}_p(E)$ were significant, then because the mixture of spin states for the fissioning ^{234}U nucleus is not the same for incident photons as it is for incident neutrons, especially as the incident neutron energy increases and brings with it larger contributions of higher partial waves

TABLE IV. Comparison of values for $\bar{\nu}_p$ at $E=8.5$ MeV.

Nucleus	Bremsstrahlung[a]	Monoenergetic photons[b]
^{233}U	2.65	2.63
^{234}U	2.56	2.71
^{237}Np	2.53	2.90
^{239}Pu	3.32	3.29

[a]From Ref. 19.
[b]Present results.

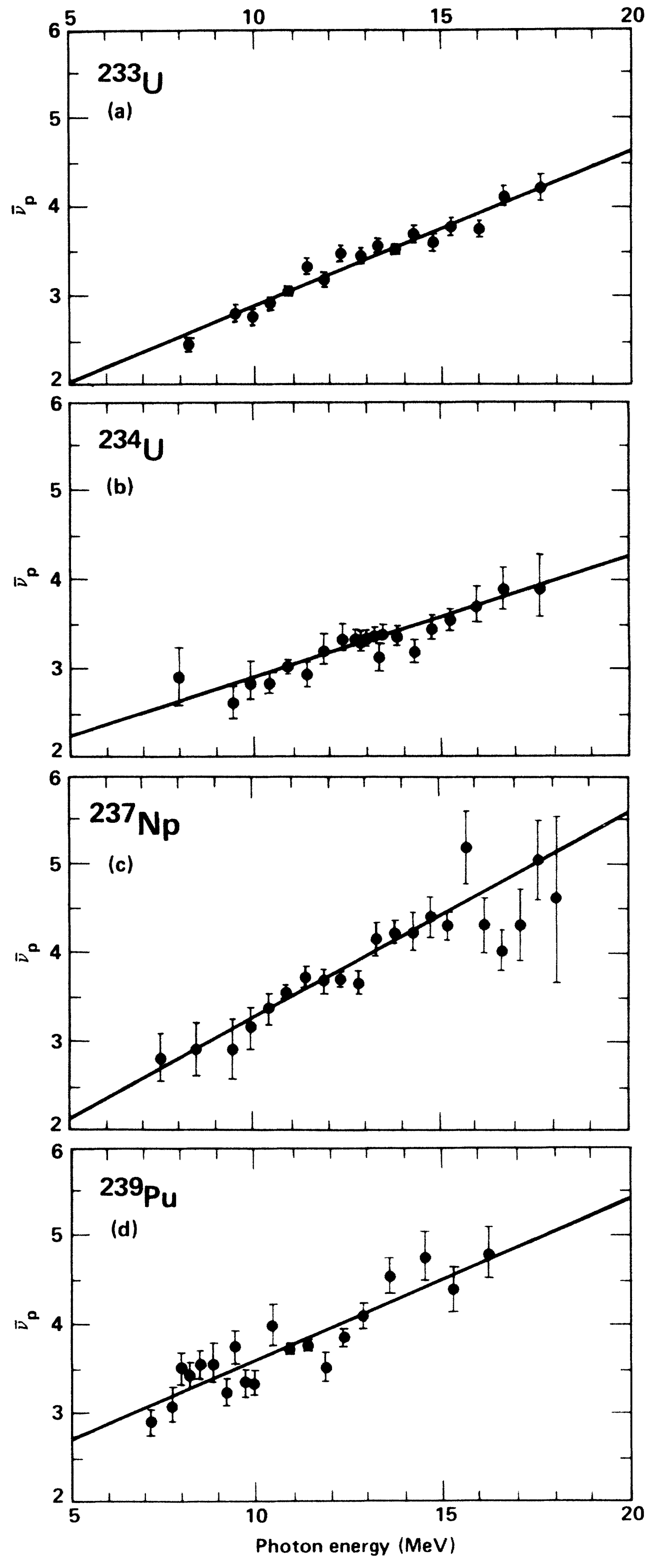

FIG. 2. Average number of prompt neutrons $\bar{\nu}_p(E)$ from the photofission of (a) ^{233}U, (b) ^{234}U, (c) ^{237}Np, and (d) ^{239}Pu measured in the present experiment (data points). The straight lines are the best least-squares fits to these data (see Table III).

TABLE V. Comparison of values for $\bar{\nu}_p$ at threshold.

Nucleus	Thermal neutrons[a]	Calculated[b]	Fit to present data
^{233}U	3.14	2.53	2.17
^{234}U	2.49	2.51	2.50
^{239}Pu	2.90	2.82	2.78

[a]From Refs. 22 (^{234}U) and 23 (^{233}U and ^{239}Pu). The results of Ref. 23 are normalized to those of Ref. 22.
[b]From Ref. 33.

(the photofission process is dominated by $E1$ transitions for all photon energies, of course), one might see a discrepancy between the two determinations of $\bar{\nu}_p$ that increases with energy. There is, in fact, a hint of this effect in the data (see Fig. 3).

B. Cross sections

The photonuclear cross sections for ^{233}U, ^{234}U, ^{237}Np, and ^{239}Pu are shown, as functions of photon energy, in Figs. 4—7, respectively. The total photonuclear cross sections

$$\sigma(\gamma,\mathrm{tot})=\sigma[(\gamma,1\mathrm{n})+(\gamma,2\mathrm{n})+(\gamma,F)] ,$$

where the total photofission cross section $\sigma(\gamma,F)$ is the sum of the first-chance photofission cross section $\sigma(\gamma,f)$ and the second-chance photofission cross section $\sigma(\gamma,\mathrm{n}f)$, are shown in Figs. 4(a), 5(a), 6(a), and 7(a). All have about the same peak cross-section value ($\approx$0.5 b) and width ($\approx$6 MeV). Also, they clearly are split in the fashion of other statically deformed nuclei.[5—7,34] All have been fitted with two-component Lorentz curves (more on this in Sec. III C). No obvious structure, other than the GDR itself, appears in these cross sections.

The single-photoneutron cross sections $\sigma(\gamma,1\mathrm{n})$ are shown in Figs. 4(b), 5(b), 6(b), and 7(b). Note that the measured $\sigma(\gamma,1\mathrm{n})$ includes $\sigma(\gamma,\mathrm{pn})$ and $\sigma(\gamma,\alpha\mathrm{n})$, but these cross sections are expected to be very small below 18 MeV because of the Coulomb barrier, not to mention the competition from the photofission channels. The size of the $(\gamma,1\mathrm{n})$ cross section varies widely for these nuclei; for ^{233}U it is considerably smaller than for the other three. The $(\gamma,1\mathrm{n})$ cross sections fall sharply above the $(\gamma,2\mathrm{n})$ thresholds, as is the case for essentially all other medium and heavy nuclei.[5,34] None of the $(\gamma,1\mathrm{n})$ cross sections (with the possible exception of that for ^{237}Np) has the double-humped shape characteristic of deformed nuclei, and thus

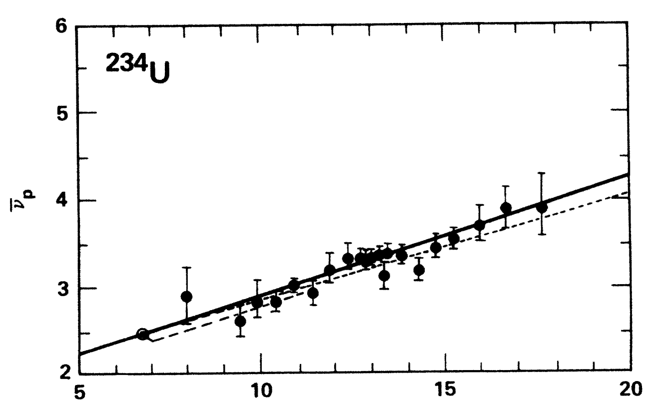

FIG. 3. Same as Fig. 2(b) for ^{234}U+γ, with the results of ^{233}U + n measurements superposed. The circled dot is the result of Ref. 22 for thermal neutrons, the long-dashed line represents the data of Ref. 21, and the short-dashed line the data of Ref. 20.

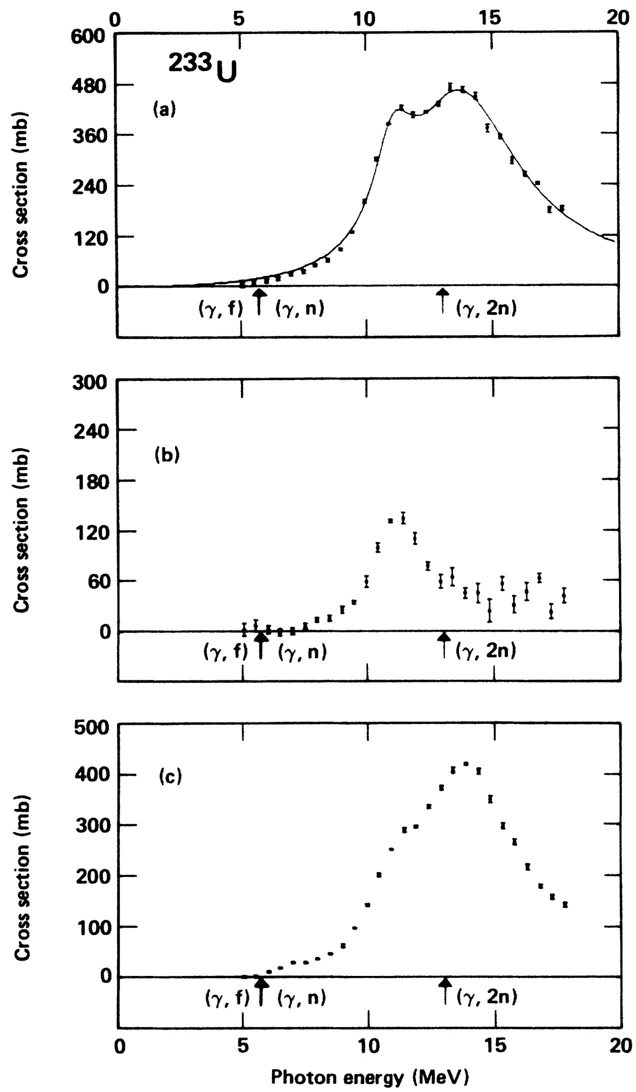

FIG. 4. Photonuclear cross sections for ^{233}U: (a) the total photonuclear cross section $\sigma(\gamma,\mathrm{tot})=\sigma[(\gamma,1\mathrm{n})+(\gamma,2\mathrm{n})+(\gamma,F)]$, together with a two-component Lorentz-curve fit [Eq. (1)] to the data in the GDR energy region (9—18 MeV); (b) the single-photoneutron cross section $\sigma(\gamma,1\mathrm{n})$; (c) the photofission cross section $\sigma(\gamma,F)=\sigma[(\gamma,f)+(\gamma,\mathrm{n}f)]$. The double-photoneutron cross section $\sigma(\gamma,2\mathrm{n})$ was measured to be consistent with zero for this nucleus (see Sec. II). The arrows in Figs. 4—11 and 14 locate the photonuclear thresholds and fission barriers taken from Refs. 24 and 4 (see Table II).

a measurement of $\sigma(\gamma,1n)$ alone (by the activation technique, for example) would not yield even a rough idea of the deformation parameters for these nuclei.

The $(\gamma,2n)$ cross sections for ^{237}Np and ^{239}Pu are shown in Figs. 6(c) and 7(c), respectively. That they are small is no surprise, because the high fissionability of these nuclei implies that most of the photonuclear strength will appear in the fission decay channel. What *is* surprising is that for both ^{233}U and ^{234}U there is *no* $(\gamma,2n)$ cross section distinguishable (within our experimental limits) from zero, even though these nuclei also have high fissionabilities. These are the only nuclei [except for the light self-conjugate nuclei having very high $(\gamma,2n)$ thresholds] which exhibit this kind of behavior.[34] This behavior is a clear indication of the power of the fission process to distort the "normal" decay pattern of the GDR.

The photofission cross sections $\sigma(\gamma,F)$ are shown in Figs. 4(c), 5(c), 6(d), and 7(d). All are large, reaching $\approx$400 mb at $\approx$14 MeV, and all show a significant (and expected) rise above the second-chance fission thresholds at 12—13 MeV. Again we notice that a measurement of

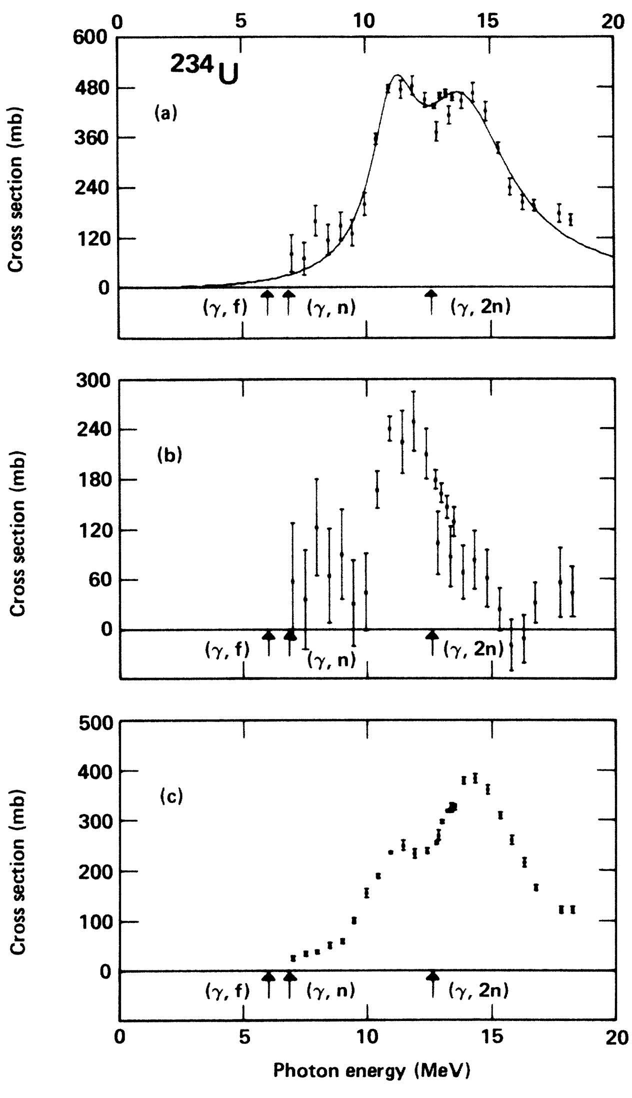

FIG. 5. Photonuclear cross sections for ^{234}U: (a) $\sigma(\gamma,\text{tot})$, with a Lorentz-curve fit; (b) $\sigma(\gamma,1n)$; (c) $\sigma(\gamma,F)$. The $(\gamma,2n)$ cross section was measured to be consistent with zero for this nucleus (see Sec. II).

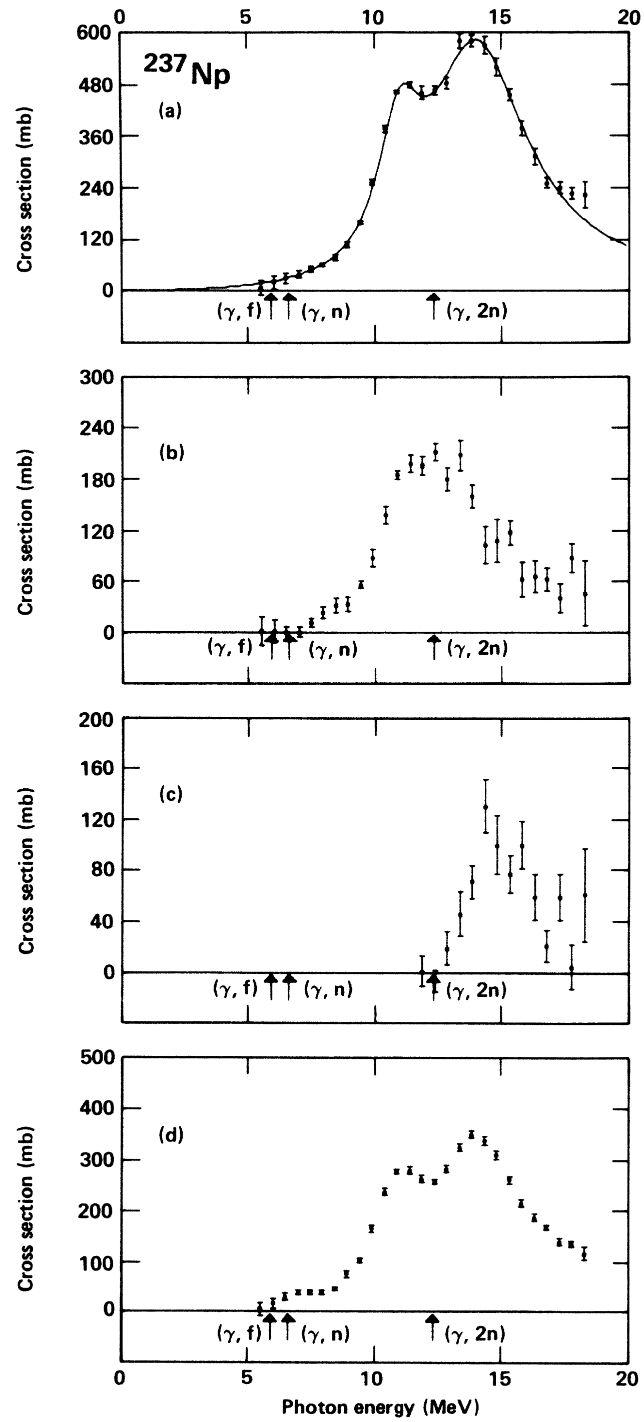

FIG. 6. Photonuclear cross sections for ^{237}Np: (a) $\sigma(\gamma,\text{tot})$, with a Lorentz-curve fit; (b) $\sigma(\gamma,1n)$; (c) $\sigma(\gamma,2n)$; (d) $\sigma(\gamma,F)$.

only one photonuclear channel would give a distorted and erroneous view of the shape of the GDR; we see that $\sigma(\gamma,F)$ alone would lead to values for the ratio of the areas R_A of the first to the second hump of the GDR that are much too small (see Sec. III C).

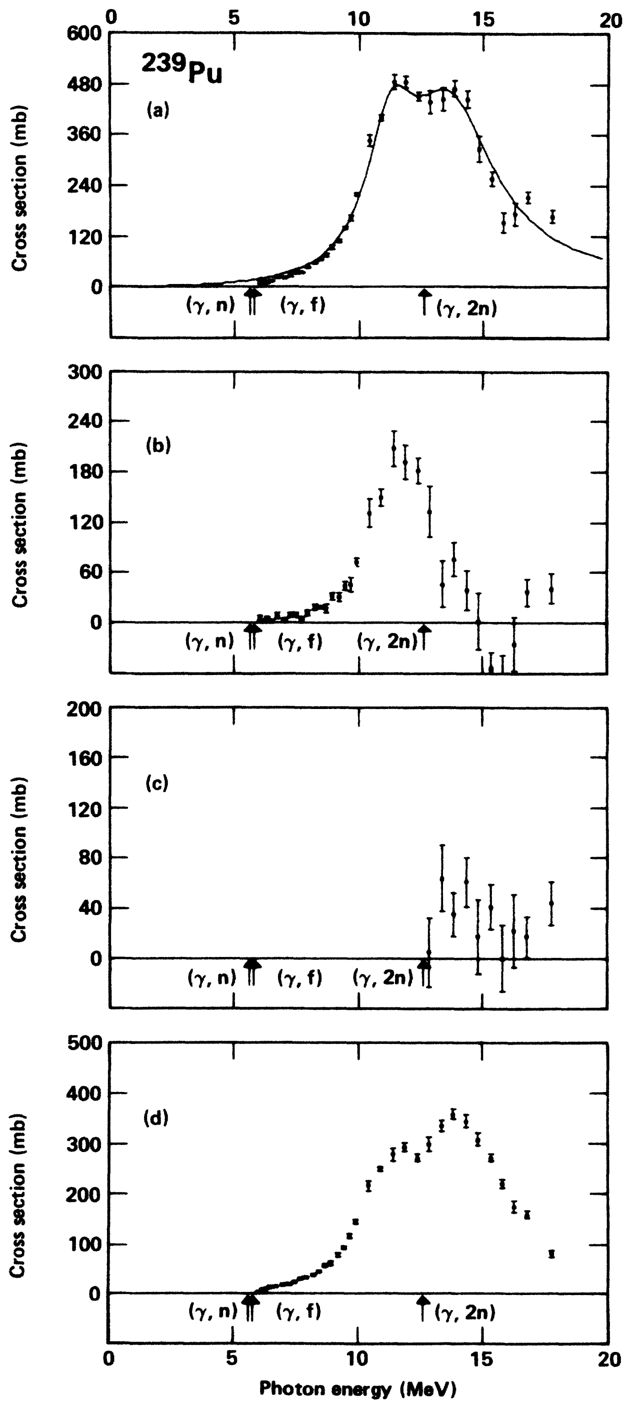

FIG. 7. Photonuclear cross sections for ^{239}Pu: (a) $\sigma(\gamma,\text{tot})$, with a Lorentz-curve fit; (b) $\sigma(\gamma,1\text{n})$; (c) $\sigma(\gamma,2\text{n})$; (d) $\sigma(\gamma,F)$.

C. Giant-resonance parameters

The classic collective description of the GDR predicts that the total photon-absorption cross section $\sigma(\gamma,\text{tot})$ for statistically deformed nuclei is characterized as the sum of two Lorentz-shaped curves,

$$\sigma(\gamma,\text{tot})=\Sigma\sigma_m(i)\Big/\left\{1+\frac{[E_\gamma^2-E_m^2(i)]^2}{E_\gamma^2\Gamma^2(i)}\right\}, \tag{1}$$

where $\sigma_m(i)$, $E_m(i)$, and $\Gamma(i)$ are the peak height, resonance energy, and full width of the ith Lorentz curve. Accordingly, the (γ,tot) cross sections in Figs. 4(a), 5(a), 6(a), and 7(a) have been fitted with two-component Lorentz curves. The fitting interval used for all four nuclei was 9–18 MeV, which includes the entire GDR region. The resulting fits to the data are shown in the figures, and the Lorentz parameters of these fitted curves are given, together with their statistical uncertainties, in Table VI.

Values of the parameters for the classified theories are given in Table VII. These include α and β, the proportionality constants characterizing the mean GDR energy E_m with mass number, and K, the nuclear symmetry energy computed from the relation

$$K=9.935\times10^{-4}\frac{A^{8/3}}{NZ}\frac{E_m(1)^2}{1-[\Gamma(1)/2E_m(1)]^2}\times\frac{\eta^{4/3}}{(1+0.018\,60\epsilon-0.033\,14\epsilon^2)^2}, \tag{2}$$

where η is the nuclear deformation parameter, defined as the ratio of the semimajor axis b to the semiminor axis a of the (prolate) deformed nucleus, and computed from the relation

$$E_m(2)/E_m(1)=0.911\eta+0.089, \tag{3}$$

and ϵ is the nuclear eccentricity, defined as $(b^2-a^2)/R^2$, where R is the radius of a sphere of equal volume (for a prolate spheroid, $R^3=a^2b$), and computed from the resulting relation

$$\epsilon=(\eta^2-1)\eta^{-2/3}. \tag{4}$$

The value for E_m for a prolate spheroid should be given by

$$E_m=[E_m(1)+2E_m(2)]/3, \tag{5}$$

two-thirds of the way from the lower- to the higher-energy peak of the GDR; this value has been adopted for all the nuclei studied here. The present values both for K and for E_m follow very well the systematics for these quantities discussed at length in Ref. 5.

Values for various nuclear shape parameters, computed from the Lorentz parameters of Table VI, are given in Table VIII. These are R_A, the area ratio defined as

$$R_A=\sigma_m(1)\Gamma(1)/\sigma_m(2)\Gamma(2) \tag{6}$$

and predicted to be one-half for prolate nuclei; η, the deformation parameter of Eq. (3); ϵ, the nuclear eccentricity of Eq. (4); β_2, a deformation parameter more commonly used than η or ϵ, defined as

TABLE VI. Parameters of Lorentz-curve fits to the GDR.[a]

Nucleus	$E_m(1)$ (MeV)	$\sigma_m(1)$ (mb)[b]	$\Gamma(1)$ (MeV)	$E_m(2)$ (MeV)	$\sigma_m(2)$ (mb)[b]	$\Gamma(2)$ (MeV)
^{233}U	11.08±0.06	221±26	1.94±0.26	13.86±0.14	433±13	5.47±0.30
^{234}U	11.13±0.10	371±36	2.26±0.38	13.94±0.16	401±22	4.46±0.47
^{237}Np	10.98±0.04	311±16	2.17±0.14	14.08±0.07	540±12	4.66±0.23
^{237}Np[c]	11.02±0.09	256±21	2.94±0.34	14.11±0.11	392±16	4.71±0.37
^{239}Pu	11.28±0.20	325±90	2.48±0.47	13.73±0.43	384±60	4.25±0.83
^{239}Pu[d]	11.01±0.14	225±31	3.22±0.45	13.95±0.17	371±23	5.38±0.41

[a]Lorentz parameters defined by Eq. (1). The fitting interval for all cases is 9—18 MeV.
[b]The uncertainties for σ_m given here are relative. The absolute uncertainties for the present data are 7%.
[c]From the data of Ref. 9.
[d]From the data of Ref. 11.

$$\beta_2=\tfrac{2}{3}(\pi/5)^{1/2}\epsilon\approx 0.53\epsilon\ , \tag{7}$$

and Q_0, the intrinsic quadrupole moment defined as

$$Q_0=\tfrac{2}{5}ZR^2\epsilon\ , \tag{8}$$

where $R=R_0A^{1/3}$ is the equivalent nuclear radius. For two of the nuclei studied here (^{233}U and ^{237}Np), R_A is not equal to the hydrodynamic prediction of one-half; rather, a value close to one-fourth is indicated in Table VIII. We have no ready explanation for this feature of the data; similar behavior occurs for nuclei on the fringes, rather than in the center, of the deformed rare-earth region.[6]

Values for Q_0 computed from Eq. (8) with R_0 taken to be 1.15 fm are given in the sixth column of Table VIII, in keeping with the results of the analysis in Ref. 7. Other determinations (by a variety of techniques) of Q_0 are listed in the last column of Table VIII. The agreement is seen to be excellent in all cases except that for ^{239}Pu, and for this case the present uncertainty [see Fig. 7(a) and Table VIII] is much larger than for the others.

D. Integrated cross sections and their moments

The integrated cross sections and their first and second energy moments measured in this experiment are given in Table IX. Up to the highest photon energy measured $E_{\gamma\,\max}$, listed in column 2 of Table IX, the integrated (γ,n), (γ,2n), (γ,F), and (γ,tot) cross sections are given in columns 3—6 and the first and second moments σ_{-1} and σ_{-2} of the total cross section in columns 7 and 8, respectively. Again it can be seen that the decay of the GDR for all of these nuclei is dominated by the fission channel (also see Sec. III F). The value of σ_{-2} is proportional to the nuclear polarizability (see Ref. 5).

In columns 3 and 4 of Table X, we compare the value of the integrated total cross section (up to $E_{\gamma\,\max}$) with the total area under the two-component Lorentz-curve fit to the GDR (integrated from zero to infinite energy) for each nucleus studied here, in TRK (Thomas-Reiche-Kuhn) sum-rule units, whose values are listed in column 2. The values listed in column 4 give an indication of the maximum amount of exchange-force enhancement of the dipole sum-rule values that might be needed to account for the GDR. The results for ^{233}U, ^{234}U, and ^{239}Pu agree with the value for ^{236}U (Ref. 7) and with the systematic result of 1.21±0.11 sum-rule units of Ref. 5, whereas the result for ^{237}Np lies higher, but is comparable to those for ^{235}U, ^{238}U, and ^{232}Th (Ref. 7).

The present experimental data for all of the integrated cross sections and their moments are shown in Figs. 8—11 in the form of running sums of the quantities plotted as functions of the photon energy up to which they are integrated. This form of displaying the integrated cross-section data is useful for information-retrieval purposes, and also shows whether the various plotted quantities approach asymptotic behavior at the highest photon energies measured. These figures show that the integrated cross sections and their moments do not approach asymptotic values, except for the (γ,1n) channel, but this merely reflects the fact that the present measurements were carried out only up to $E_{\gamma\,\max}\approx 18$ MeV.

TABLE VII. Parameters for classical theories.[a]

Nucleus	E_m[b]	α[c]	β[d]	K[e]
^{233}U	12.94	79.6	32.1	27.7
^{234}U	13.00	80.1	32.3	27.7
^{237}Np	13.04	80.7	32.5	28.2
^{239}Pu	12.92	80.2	32.2	27.7

[a]All quantities given in MeV.
[b]Mean energy of the GDR, defined by Eq. (5).
[c]Hydrodynamic parameter, defined by $E_m=\alpha A^{-1/3}$.
[d]Collective parameter, defined by $E_m=\beta A^{-1/6}$.
[e]Nuclear symmetry energy, computed from Eq. (2).

E. Comparison with other experiments

1. The GDR energy region

Measurements of photofission and photoneutron yield cross sections made prior to the 1970s are neither accurate nor detailed enough to be compared profitably with the present data. The annihilation-photon experiment of Veyssière *et al.*[9] was performed in much the same way as the present work, except that the authors of Ref. 9 assumed values for $\bar{\nu}_p(E)$ instead of measuring them. For

TABLE VIII. Nuclear shape parameters.

Nucleus	R_A [a]	η [b]	ϵ [c]	β_2 [d]	Q_0 (b) [e]	Q_0 (b)
^{233}U	0.18	1.275	0.533	0.282	9.8±0.5	10.3±0.3 [f]
^{234}U	0.47	1.277	0.536	0.284	9.9±0.8	10.0±0.4 [g]
^{237}Np	0.27	1.310	0.598	0.317	11.3±0.4	{ 9.8±0.9 [b] 12.0±1.1 [h]
^{239}Pu	0.49	1.238	0.463	0.245	8.9±1.8	12.0±0.3 [f]

[a] Area ratio, defined by Eq. (6).
[b] Deformation parameter, computed from Eq. (3).
[c] Nuclear eccentricity, computed from Eq. (4).
[d] Deformation parameter, computed from Eq. (7).
[e] Intrinsic quadrupole moment, computed from Eq. (8), with R_0 taken to be 1.15 fm.
[f] From Ref. 35.
[g] From Ref. 36.
[h] From Ref. 37.

^{237}Np, the values assumed by Veyssière *et al.*[9] up to ≈ 14 MeV lie substantially higher than our measured ones. This results in lower values for the cross sections in much of the GDR region; in terms of integrated total cross section, the value of Ref. 9 for ^{237}Np is about 25% lower than the present result, although the shapes of the partial cross sections are not very different. Another way to compare the present data with those of Ref. 9 is to compare the Lorentz parameters of the latter when they are fitted in the same way as the former. These parameters all are listed in Table VI. Of course, if the data of Ref. 9 were reanalyzed using our measured values for $\bar{\nu}_p(E)$, these parameters would change somewhat.

The photon-absorption measurement of $\sigma(\gamma,\text{tot})$ of Gurevich *et al.*[11] yields a result for ^{239}Pu that, like their results for ^{235}U, ^{236}U, and ^{232}Th (see Ref. 7), is about 10% smaller than the present result. The uncertainties quoted in Ref. 11 range from 10% to 13%, which, added to the 7% uncertainty for the present measurement, place the two sets of data in agreement within the experimental limits. The overall shapes of the cross sections of Ref. 11 are likewise similar to the present results, especially for ^{238}U; the Lorentz parameters for the ^{239}Pu data of Ref. 11 also are given for comparison purposes in Table VI. However, the subtraction of the large atomic absorption (50–100 times the photonuclear absorption) for these high-Z atoms makes the total photon-absorption measurements difficult.

2. *The low-energy region*

The photofission cross sections for the energy region below 10 MeV are plotted in Fig. 12 with an expanded cross-section scale so that the details of the data can be seen clearly. For comparison, all of the other low-energy photofission data for these nuclei also are shown in Fig. 12. Although comparison of the present results with cross-section data obtained by unfolding bremsstrahlung spectra yields satisfactory agreement, most bremsstrahlung experiments were not undertaken to obtain absolute cross sections, but rather to measure the angular distributions of the fission fragments or the cross-section shapes at very low energies. In particular, the results of Katz *et al.*,[10] Ostapenko *et al.*,[13] and Shapiro and Stubbins[17] for ^{233}U, ^{237}Np, and ^{239}Pu are in reasonable agreement with the present data. The ^{234}U data of Lindgren *et al.*[14,15] lie below the energy range of the present data for that nucleus.

The results of high-resolution mononenergetic-photon measurements performed with nuclear gamma rays agree with the present data for some cases, but do not for others. The cross sections reported by Huizenga *et al.*[12] for ^{233}U, ^{234}U, and ^{237}Np tend to lie higher than ours, although some data points agree quite well. There are serious discrepancies between our results and many of the data points of Geraldo *et al.*[16] for ^{237}Np and of Dragnev *et al.*[18] for ^{239}Pu. However, these measurements are of

TABLE IX. Integrated cross sections[a] and their moments.[b,c]

Nucleus	$E_{\gamma\,\max}$ (MeV)	$\sigma_{\rm int}(\gamma,{\rm n})$ (MeV b)	$\sigma_{\rm int}(\gamma,2{\rm n})$ (MeV b)	$\sigma_{\rm int}(\gamma,F)$ (MeV b)	$\sigma_{\rm int}(\gamma,{\rm tot})$ (MeV b)	$\sigma_{-1}(\gamma,{\rm tot})$ (mb)	$\sigma_{-2}(\gamma,{\rm tot})$ (mb MeV^{-1})
^{233}U	17.8	0.58		2.44	3.02	239	19.6
^{234}U	18.3	1.06		2.26	3.32	270	23.3
^{237}Np	18.3	1.17	0.35	2.28	3.80	298	24.4
^{239}Pu	17.8	0.63	0.15	2.15	2.93	235	19.6

[a] $\sigma_{\rm int}(\gamma,x)=\int \sigma(\gamma,x)dE$, integrated from threshold to $E_{\gamma\,\max}$.
[b] $\sigma_{-1}(\gamma,{\rm tot})=\int \sigma(\gamma,{\rm tot})E^{-1}dE$, integrated from threshold to $E_{\gamma\,\max}$.
[c] $\sigma_{-2}(\gamma,{\rm tot})=\int \sigma(\gamma,{\rm tot})E^{-2}dE$, integrated from threshold to $E_{\gamma\,\max}$.

TABLE X. Integrated total cross sections.

Nucleus	$0.060NZ/A$ (MeV b)	$\frac{\sigma_{int}(\gamma,\mathrm{tot})}{0.060NZ/A}$	$\frac{(\pi/2)[\sigma_m(1)\Gamma(1)+\sigma_m(2)\Gamma(2)]}{0.060NZ/A}$
^{233}U	3.340	0.91[a]	1.32
^{234}U	3.350	0.99[b]	1.23
^{237}Np	3.390	1.12[b]	1.48
^{239}Pu	3.422	0.86[a]	1.12

[a] $E_{\gamma\,\max}=17.8$ MeV.
[b] $E_{\gamma\,\max}=18.3$ MeV.

such high resolution (comparable to or smaller than the spacing between levels in the compound nucleus) that the data points measured could easily coincide with peaks or valleys in the underlying fine structure of the cross sections, so that direct comparison with the present data is not very enlightening.

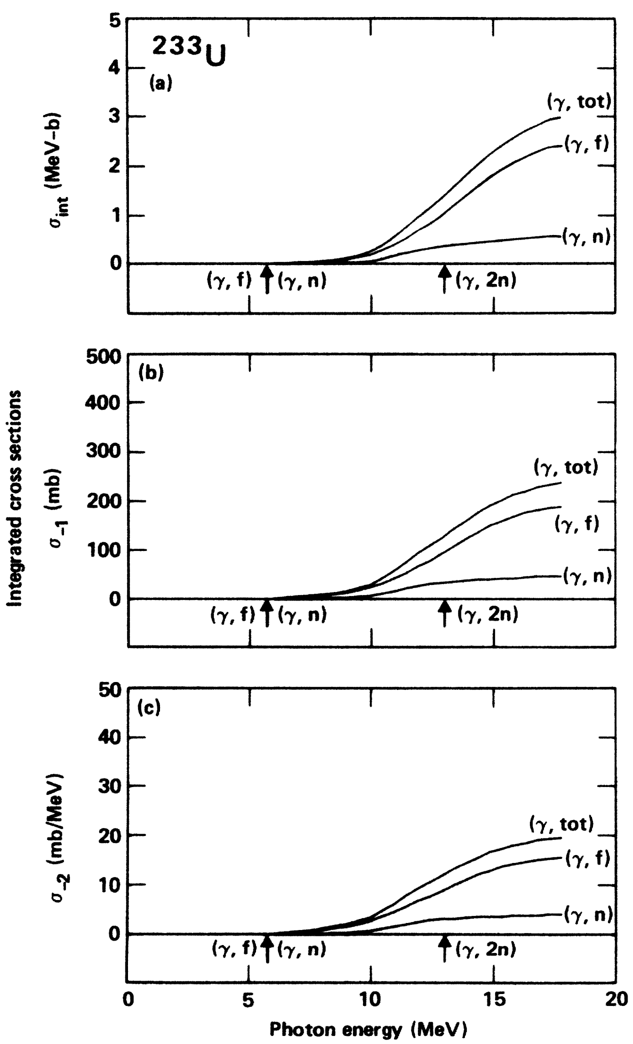

FIG. 8. Running sums of the integrated cross sections and their moments, plotted vs the upper-energy limit of integration for ^{233}U: (a) integrated cross sections σ_{int} for (γ,tot), $(\gamma,1\mathrm{n})$, and (γ,F); (b) first moment of the integrated cross sections, σ_{-1}; (c) second moment of the integrated cross sections, σ_{-2}.

F. Neutron and fission probabilities

The important branching ratio of the neutron-emission width to the fission width Γ_n/Γ_f can be determined at low excitation energies directly from $\sigma(\gamma,\mathrm{n})/\sigma(\gamma,F)$ because only first-chance photofission reactions are energetically possible. At higher energies, however, second-chance photofission reactions become possible (the

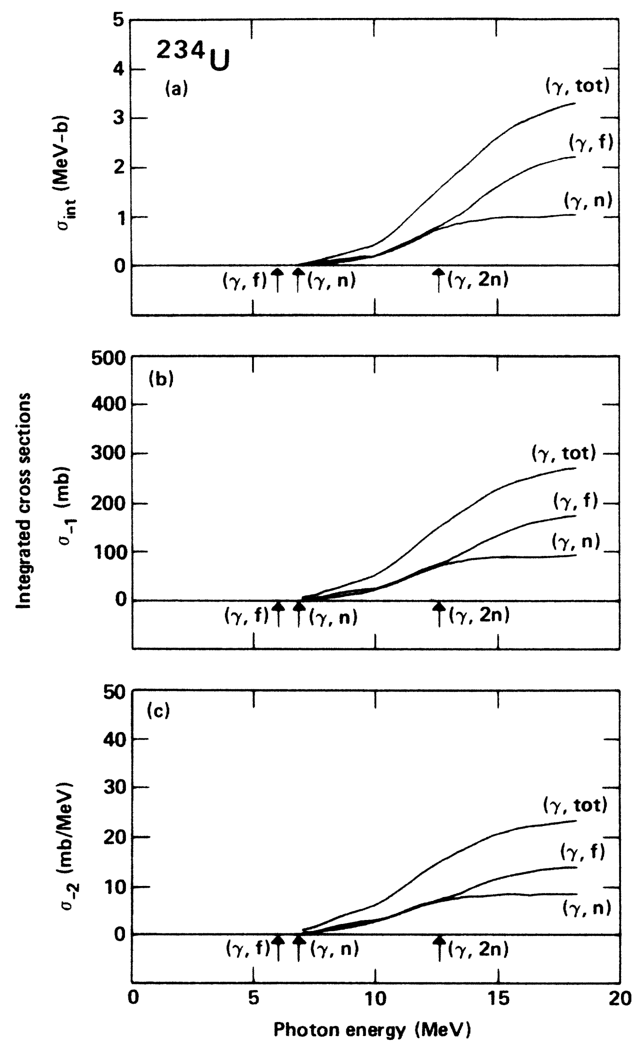

FIG. 9. Running sums of integrated cross sections and moments for ^{234}U: (a) σ_{int} for (γ,tot), $(\gamma,1\mathrm{n})$, and (γ,F); (b) σ_{-1}; (c) σ_{-2}.

TABLE XI. Fissionabilities.

Nucleus	Z^2/A	$\frac{\sigma_{\mathrm{int}}(\gamma,F)}{\sigma_{\mathrm{int}}(\gamma,\mathrm{tot})}$	Γ_n/Γ_f
^{232}Th	34.91	0.11	15
^{238}U	35.56	0.30	3.9
^{236}U	35.86	0.46	2.1
^{235}U	36.02	0.62	1.4
^{234}U	36.17	0.68	0.99
^{233}U	36.33	0.81	0.49
^{237}Np	36.49	0.60	0.68
^{239}Pu	36.97	0.74	0.62

second-chance fission barriers generally lie between 12 and 13 MeV), and one must separate these two components in order to determine Γ_n/Γ_f. Details of how this has been done previously are given in Ref. 7. Poor statistics or large multiplication corrections make this procedure statistically uncertain for the nuclei studied here. Nevertheless, for all of the nuclei that we have studied, because Γ_n/Γ_f reaches an asymptotic value in the energy region above 9–10 MeV, the values for Γ_n/Γ_f determined at 11 MeV should be characteristic of all of these nuclei. These values for Γ_n/Γ_f are plotted in Fig. 13 as a function of the nuclear fissionability Z^2/A (see Ref. 4, pp. 16 and 17). Also shown in Fig. 13 are values for Γ_n/Γ_f deduced from our previous photonuclear data and those of Veyssière *et al.*[9] and from the charged-particle-induced fission data of Gavron *et al.*[38] The open symbols in the figure, other than those for the charged-particle data, represent previous values for Γ_n/Γ_f obtained from $\sigma(\gamma,\mathrm{n})/\sigma(\gamma,f)$, while the solid symbols represent values for the target-minus-one-neutron nucleus obtained from $\sigma(\gamma,2\mathrm{n})/\sigma(\gamma,\mathrm{n}f)$. [The values for $\sigma(\gamma,\mathrm{n}f)$ used in Ref. 9 were obtained by an extrapolation procedure rather than by a direct determination.] The present results are shown in Fig. 13 as the circled dots.

Figure 13 shows that the values for Γ_n/Γ_f decrease

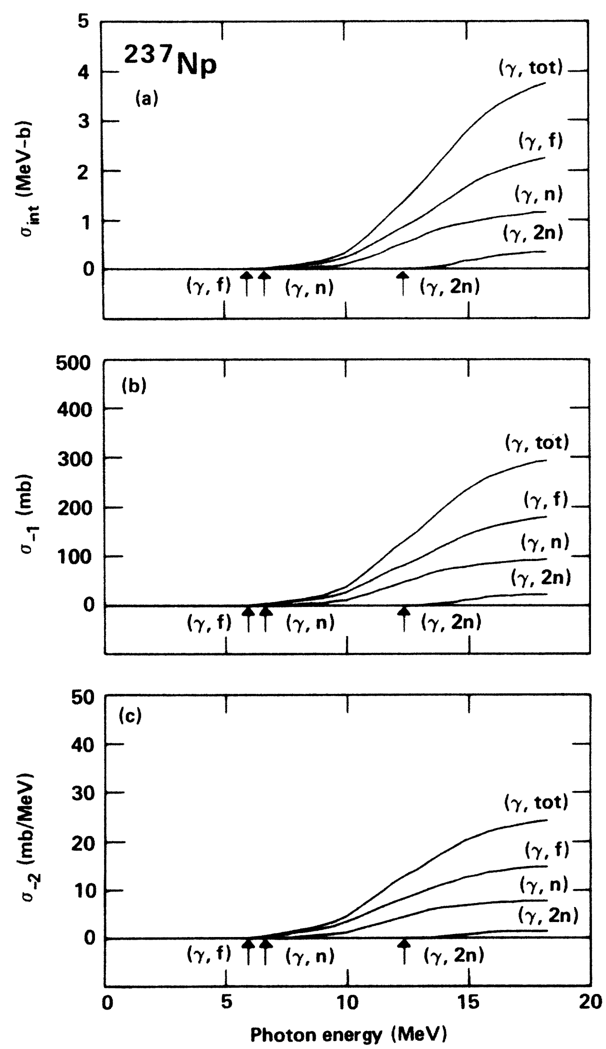

FIG. 10. Running sums of integrated cross sections and moments for ^{237}Np: (a) σ_{int} for (γ,tot), $(\gamma,1\mathrm{n})$, $(\gamma,2\mathrm{n})$, and (γ,F); (b) σ_{-1}; (c) σ_{-2}.

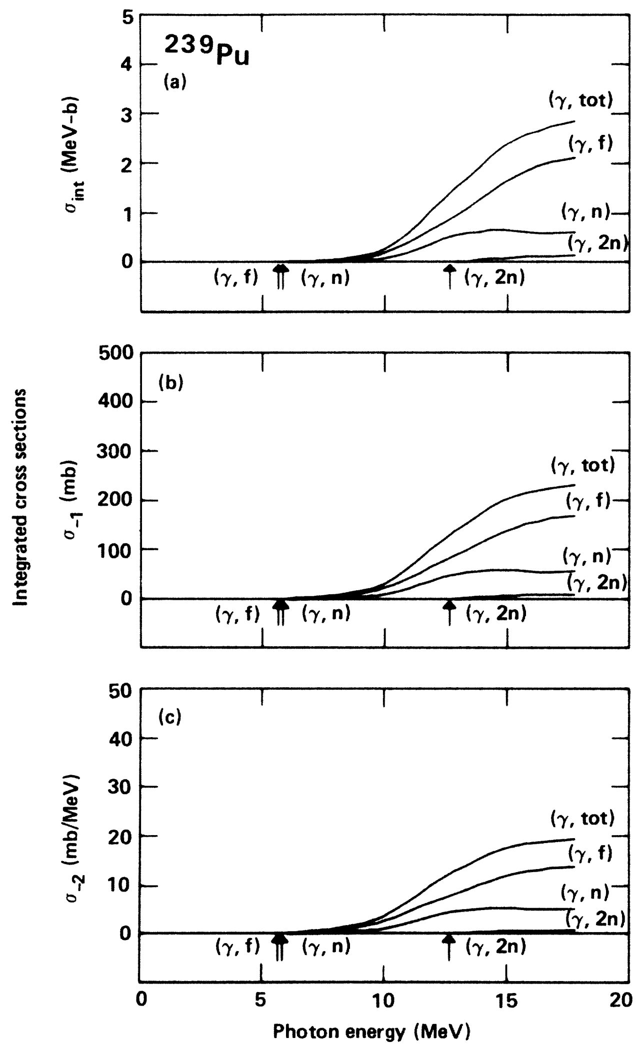

FIG. 11. Running sums of integrated cross sections and moments for ^{239}Pu: (a) σ_{int} for (γ,tot), $(\gamma,1\mathrm{n})$, $(\gamma,2\mathrm{n})$, and (γ,F); (b) σ_{-1}; (c) σ_{-2}.

more or less exponentially with the fissionability of the nucleus. The deviation from an exponential decrease at the higher values of Z^2/A probably shows the need for a surface-symmetry correction term to the fissionability.[39] Figure 13 also shows that the present value for Γ_n/Γ_f from $\sigma(\gamma,n)/\sigma(\gamma,f)$ for ^{234}U coincides with our previous value from $\sigma(\gamma,2n)/\sigma(\gamma,nf)$ for ^{235}U, and that our previous values for Γ_n/Γ_f from $\sigma(\gamma,n)/\sigma(\gamma,f)$ for ^{235}U and from $\sigma(\gamma,2n)/\sigma(\gamma,nf)$ for ^{236}U also are in excellent agreement. This agreement demonstrates an important internal consistency in the experimental data.

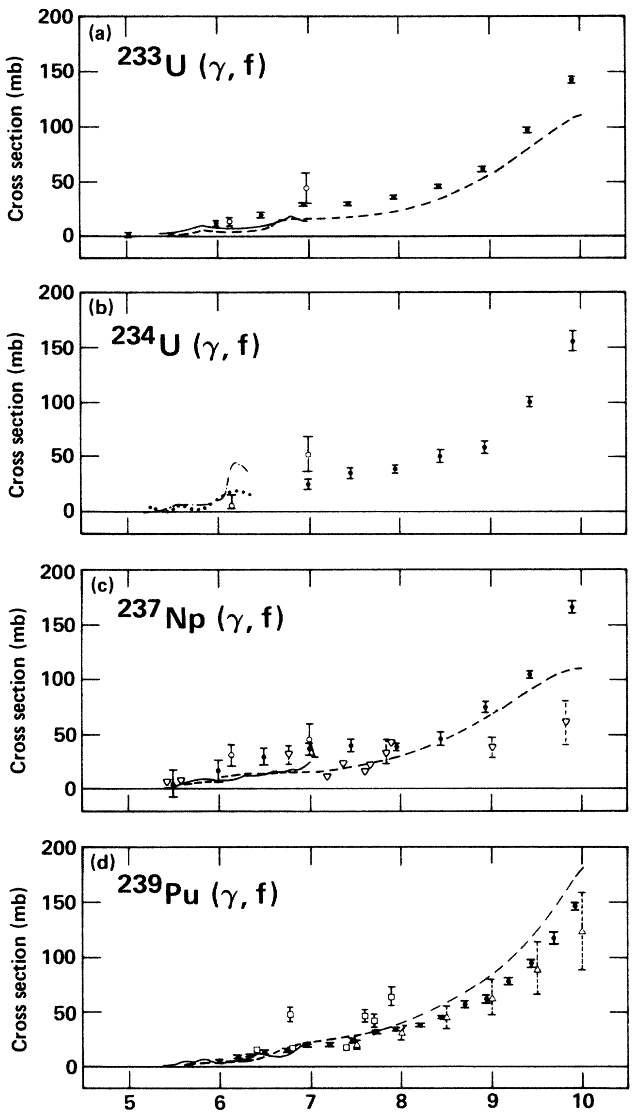

FIG. 12. Low-energy photofission cross sections $\sigma(\gamma,f)$ for (a) ^{233}U: solid date points—present work, open data points—Ref. 12, solid curve—Ref. 13, dashed curve—Ref. 10; (b) ^{234}U: solid data points—present work, open data points—Ref. 12, dotted curve—Ref. 14, dotted-dashed curve—Ref. 15; (c) ^{237}Np: solid data points—present work, open circles—Ref. 12, open triangles—Ref. 16, solid curve—Ref. 13, dashed curve—Ref. 10; and (d) ^{239}Pu: solid data points—present work, open squares—Ref. 18, open triangles—Ref. 17, solid curve—Ref. 13, dashed curve—Ref. 10.

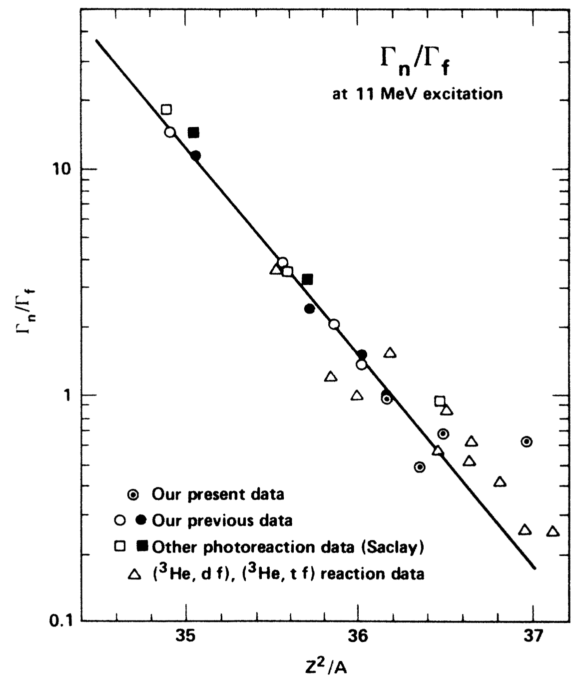

FIG. 13. Neutron-to-fission branching ratio Γ_n/Γ_f at 11-MeV excitation energy vs nuclear fissionability Z^2/A: circled dots—present work, from $\sigma(\gamma,n)/\sigma(\gamma,f)$; open circles—work of Ref. 7, from $\sigma(\gamma,n)/\sigma(\gamma,f)$; solid circles—work of Ref. 7, from $\sigma(\gamma,2n)/\sigma(\gamma,nf)$; open squares—work of Ref. 9, from $\sigma(\gamma,n)/\sigma(\gamma,f)$; solid squares—work of Ref. 9, from $\sigma(\gamma,2n)/\sigma(\gamma,nf)$; triangles—work of Ref. 38, from (^{3}He,df) and (^{3}He,tf) reactions.

The values of Γ_n/Γ_f for all of the eight actinide nuclei that we have studied are contrasted in Table XI with the ratio of integrated photofission and total photonuclear cross sections. As the fissionability Z^2/A increases, $\sigma_{\rm int}(\gamma,F)/\sigma_{\rm int}(\gamma,{\rm tot})$ increases sharply and Γ_n/Γ_f decreases sharply, with a slight irregularity near $Z^2/A=36.3$ (^{233}U), thus demonstrating once again the importance of the fissionability in determining the decay properties of the compound nucleus.

Another important nuclear parameter is the fission probability P_f and its energy dependence. We obtain values for $P_f(E)$ here by dividing the measured (γ,f) cross sections by the values of the two-component Lorentz-curve fits to the GDR obtained in Sec. III C. This procedure smoothes the data in a meaningful way, because the representation of the total photonuclear cross section by such a curve follows the reasonable (for these nuclei) prescription of the hydrodynamic model. The values for $P_f(E)$ so obtained are shown in Figs. 14(a)–14(d) for ^{233}U, ^{234}U, ^{237}Np, and ^{239}Pu, respectively. The values of P_f near 7–8 MeV for ^{234}U and ^{237}Np are in reasonable agreement with those obtained from charged-particle-induced fission by Britt and collaborators.[38,40] The heights of the fission barriers are related closely to the shapes of these P_f—versus—excitation-energy curves,

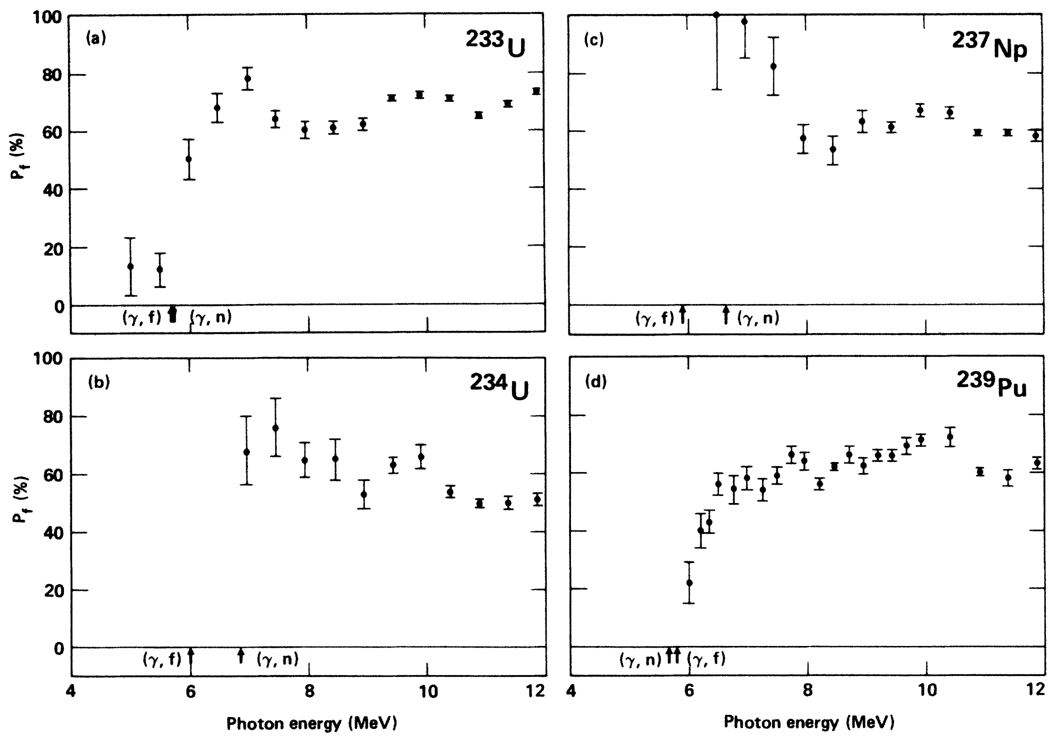

FIG. 14. Fission probability $P_f(E)$ obtained from the ratio of $\sigma(\gamma,f)$ and the value at each energy of the two-component Lorentz-curve fits to the GDR shown in Figs. 4—7 for (a) ^{233}U, (b) ^{234}U, (c) ^{237}Np, and (d) ^{239}Pu.

the height of the inner barrier to the shape near threshold, and that of the outer barrier to the asymptotic value. Further discussion of this subject can be found in Refs. 7 and 38. Here, we only wish to point out that the asymptotic values $P_{f,a}$ are determined here much better than those for the threshold region, and are all large: $P_{f,a}=0.7$, 0.5, 0.6, and 0.6 for ^{233}U, ^{234}U, ^{237}Np, and ^{239}Pu, respectively.

IV. SUMMARY

All of the major photonuclear cross sections have been measured for the four actinide nuclei ^{233}U, ^{234}U, ^{237}Np, and ^{239}Pu (Sec. III B, Figs. 4—7). The (γ,2n) cross sections for ^{233}U and ^{234}U are found to be consistent with zero up to the maximum photon energy used (≈ 18 MeV). The sum of the measured partial cross sections $\sigma(\gamma,1n)$, $\sigma(\gamma,2n)$, and $\sigma(\gamma,F)$ is a good approximation to the total photonuclear cross section and varies little from case to case within the range of nuclei studied here, thus making possible the analysis of the total cross sections by means of the semiclassical hydrodynamic model. Nuclear parameters extracted by this procedure (Sec. III C) include giant-resonance parameters (Table VI), nuclear symmetry energies (Table VII), and nuclear shape parameters (Table VIII). The integrated cross sections and their moments (Sec. III D, Figs. 8—11, and Tables IX and X) produce no unexpected results when compared with sum-rule predictions.

Properties of the nuclear fission process which have been measured include the average number of prompt neutrons per photofission $\bar{\nu}_p(E)$ and the associated neutron-multiplicity width parameter $\Sigma(E)$ (Sec. III A, Fig. 2, and Table III). These quantities are compared with other data (Fig. 3 and Tables IV and V); the $\bar{\nu}_p(E)$ data for $^{234}\text{U}+\gamma$ are found to be reasonably close both in magnitude and energy dependence to those for $^{233}\text{U}+\text{n}$. The low-energy photofission cross sections are found to increase smoothly and monotonically with energy, in agreement with most previous results (Fig. 12). The measured ratio of neutron and fission widths Γ_n/Γ_f fits the general exponential fall with fissionability Z^2/A, in keeping with previous results (Fig. 13 and Table XI). Finally, absolute fission probabilities $P_f(E)$ were extracted from the data and are determined well in the asymptotic region (Fig. 14).

ACKNOWLEDGMENTS

We thank the staff of the Lawrence Livermore National Laboratory Electron-Positron Linear Accelerator for their expert help, Dr. T. F. Godlove for his help in the early stages of the experiment, Mr. J. B. Berman for his help with the multiplication-correction calculations, and Dr. R. Bergère and Dr. B. A. Tulupov for sending us their data in numerical form. This work was performed under the auspices of the U.S. Department of Energy. A preliminary account of it has appeared as Ref. 41.

[1]A. Bohr, *Proceedings of the International Conference on the Peaceful Uses of Atomic Energy, Geneva, 1955* (United Nations, New York, 1956), Vol. 2, p. 151.

[2]J. R. Huizenga and H. C. Britt, in *Proceedings of the International Conference on Photonuclear Reactions and Applications,* edited by B. L. Berman (Lawrence Livermore National Laboratory, Livermore, 1973), p. 833.

[3]B. S. Bhandari and I. C. Nascimento, Nucl. Sci. Eng. **60**, 19 (1976).

[4]R. Vandenbosch and J. R. Huizenga, *Nuclear Fission* (Academic, New York, 1973).

[5]B. L. Berman and S. C. Fultz, Rev. Mod. Phys. **47**, 713 (1975).

[6]B. L. Berman, M. A. Kelly, R. L. Bramblett, J. T. Caldwell, H. S. Davis, and S. C. Fultz, Phys. Rev. **185**, 1576 (1969).

[7]J. T. Caldwell, E. J. Dowdy, B. L. Berman, R. A. Alvarez, and P. Meyer, Phys. Rev. C **21**, 1215 (1980).

[8]J. T. Caldwell, E. J. Dowdy, R. A. Alvarez, B. L. Berman, and P. Meyer, Nucl. Sci. Eng. **73**, 153 (1980).

[9]A. Veyssière, H. Beil, R. Bergère, P. Carlos, A. Leprêtre, and K. Kernbach, Nucl. Phys. **A199**, 45 (1973).

[10]L. Katz, A. P. Baerg, and F. Brown, *Proceedings of the Second International Conference on the Peaceful Uses of Atomic Energy* (United Nations, Geneva, 1958), Vol. 15, p. 188.

[11]G. M. Gurevich, L. E. Lazareva, V. M. Mazur, G. V. Solodukhov, and B. A. Tulupov, Nucl. Phys. **A273**, 326 (1976).

[12]J. R. Huizenga, K. M. Clarke, J. E. Gindler, and R. Vandenbosch, Nucl. Phys. **34**, 439 (1962).

[13]Yu. B. Ostapenko, G. N. Smirenkin, A. S. Soldatov, V. E. Zhuchko, and Yu. M. Tsipenyuk, submitted to Vopr. At. Nauk. Tekh. Ser.: Yad. Konst.

[14]L. J. Lindgren, A. Alm, and A. Sandell, Nucl. Phys. **A298**, 43 (1978).

[15]L. J. Lindgren, A. S. Soldatov, and Yu. M. Tsipenyuk, Sov. J. Nucl. Phys. **32**, 173 (1980).

[16]L. P. Geraldo, L. A. Vinhas, and M. T. F. Cesar, Nucl. Sci. Eng. **89**, 150 (1985).

[17]A. Shapiro and W. F. Stubbins, Nucl. Sci. Eng. **45**, 47 (1971).

[18]T. Dragnev, E. Dermendjiev, N. Kalinkova, N. Kashukeev, N. Tschikov, and N. Yaneva, Progress Report on Nuclear Data Activities in Bulgaria, 1973, p. 42.

[19]J. T. Caldwell and E. J. Dowdy, Nucl. Sci. Eng. **56**, 179 (1975).

[20]F. Manero and V. A. Konshin, At. Energy Rev. **10**, 637 (1972).

[21]J. W. Boldeman, W. K. Bertram, and R. L. Walsh, Nucl. Phys. **A265**, 337 (1976).

[22]R. Gwin, R. R. Spencer, and R. W. Ingle, Nucl. Sci. Eng. **87**, 381 (1984).

[23]A. H. Jaffey and J. L. Lerner, Nucl. Phys. **A145**, 1 (1970).

[24]A. H. Wapstra and K. Bos, At. Data Nucl. Data Tables **19**, 215 (1977).

[25]S. C. Fultz, R. L. Bramblett, J. T. Caldwell, and R. R. Harvey, Phys. Rev. **133**, B1149 (1964).

[26]S. C. Fultz, R. A. Alvarez, B. L. Berman, and P. Meyer, Phys. Rev. C **10**, 608 (1974).

[27]D. D. Faul, B. L. Berman, P. Meyer, and D. L. Olson, Phys. Rev. C **24**, 849 (1981).

[28]R. L. Bramblett, J. T. Caldwell, B. L. Berman, R. R. Harvey, and S. C. Fultz, Phys. Rev. **148**, 1198 (1966).

[29]R. E. Sund, V. V. Verbinski, H. Weber, and L. A. Kull, Phys. Rev. C **2**, 1129 (1970).

[30]H. Beil, R. Bergère, P. Carlos, A. Leprêtre, A. Veyssière, and A. Parlag, Nucl. Phys. **A172**, 426 (1971).

[31]L. M. Young, Ph.D. thesis, University of Illinois, 1972 (unpublished).

[32]B. L. Berman, R. E. Pywell, M. N. Thompson, K. G. McNeill, J. W. Jury, and J. G. Woodworth, Bull. Am. Phys. Soc. **31**, 855 (1986).

[33]T. Yamamoto and K. Sugiyama, Ann. Nucl. Energy **5**, 613 (1978).

[34]S. S. Dietrich and B. L. Berman, At. Data Nucl. Data Tables (to be published).

[35]S. A. DeWit, G. Backenstoss, C. Daum, J. C. Sens, and H. L. Acker, Nucl. Phys. **87**, 657 (1967).

[36]P. H. Stelson and L. Grodzins, Nucl. Data A **1**, 21 (1965).

[37]J. O. Newton, Nucl. Phys. **5**, 218 (1958).

[38]A. Gavron, H. C. Britt, E. Konecny, J. Weber, and J. B. Wilhelmy, Phys. Rev. C **13**, 2374 (1976).

[39]W. J. Swiatecki, private communication.

[40]B. B. Back, O. Hansen, H. C. Britt, and J. C. Garrett, Phys. Rev. C **9**, 1924 (1974).

[41]B. L. Berman, J. T. Caldwell, E. J. Dowdy, S. S. Dietrich, P. Meyer, and R. A. Alvarez, Bull. Am. Phys. Soc. **31**, 855 (1986).